Precise size separation of water-soluble red-to-near-infrared-luminescent silicon quantum dots by gel electrophoresis

Fujii, Minoru
Minamia, Akiko
Sugimoto, Hiroshi

(Citation)
Nanoscale,12(16):9266-9271

(Issue Date)
2020

(Resource Type)
journal article

(Version)
Accepted Manuscript

ARTICLE

Precise size separation of water-soluble red-to-near-infrared-luminescent silicon quantum dots by gel electrophoresis

Received 00th January 20xx,
Accepted 00th January 20xx

DOI: 10.1039/x0xx00000x

Minoru Fujii,*[a] Akiko Minami [a] and Hiroshi Sugimoto [a]

A gel electrophoresis, which is a standard method for separation and analysis of macromolecules such as DNA, RNA and proteins, is applied for the first time to silicon (Si) quantum dots (QDs) for the size separation. In the Si QDs studied, boron (B) and phosphorus (P) are simultaneously doped. The codoping induces negative potential on the surface of a Si QD and makes it dispersible in water. Si QDs with different B and P concentrations and grown at different temperatures (950°C - 1200°C) are studied. It is shown that a native polyacrylamide gel electrophoresis can separate codoped Si QDs by size. The capability of gel electrophoresis to immobilize size-separated QDs in a solid matrix makes detailed analyses of size-purified Si QDs possible. For example, photoluminescence (PL) studies of dried gel of Si QDs grown at 1100°C demonstrate that a PL spectrum of a Si QDs solution with the PL maximum around 1.4 eV can be separated into more than 15 spectra with the PL maximum changing from 1.2 to 1.8 eV depending on the migration distance. It is found that the relation between the PL peak energy and the migration distance depends on the growth temperature of Si QDs as well as the B and P concentration. For all the samples with different impurity concentrations and grown at different temperatures, a clear trend is observed in the relation between the full width at half maximum (FWHM) and the peak energy of the PL spectra in a wide energy range. The FWHM increases with increasing the peak energy and it is nearly twice larger than those observed for undoped Si QDs. The large PL FWHM of codoped Si QDs suggests that excitons are further localized in codoped Si QDs due to the existence of charged impurities.

Introduction

A colloidal solution of silicon (Si) quantum dots (QDs) exhibits size-dependent luminescence in the red to near infrared (NIR) wavelength ranges [1-5] and is considered to be a material for fluorescence labels in bioimaging [6-9] and biosensing [10, 11]. Si QDs are also considered to be a promising material for luminescent solar concentrator [12, 13], which converts ultraviolet (UV) photons absorbed by Si QDs dispersed in a polymer window glass into NIR photons and guides the NIR photons to solar cells attached to the peripheral of the window glass.

Colloidal solutions of red to NIR luminescent Si QDs have been produced by plasma decomposition of silane[1] and by thermal disproportionation of oxygen-deficient (Si-rich) silica (SiO_x (x<2)) or polymers like hydrogen silsesquioxane[3, 14]. In both methods, as-prepared samples have size distributions, which cause inhomogeneous broadening of the luminescence spectra. In any applications utilizing fluorescence of QDs, narrowing the size distribution is crucial. A wide size distribution not only broadens the luminescence spectra, but also deteriorates the quantum yields via energy transfer from a smaller (wider band gap) QD to a larger (smaller band gap) one in the size distribution, if dense films or solids of QDs are produced from the solution; the energy migration increases the chance that excitons are captured by a dark non-luminescing QD. Furthermore, purifying the size and lifting inhomogeneous broadening of physical quantities is important for the study of the fundamental physics.

If QDs are dispersed in solution, various size separation processes can be applied. In a density gradient ultracentrifugation process, a solution of QDs is overlaid onto a density gradient medium in a tube and it is centrifuged. A solution with a size gradient is obtained [15-20]. Another more widely used method for the size separation of QDs is a size-selective precipitation process, which repeats precipitation and removal of a sub-group of largest QDs in a size distribution by repeatedly adding a small amount of poor solvent in a QD-dispersed solution[21-24]. In the case of organic-capped Si QDs dispersed in nonpolar solvents, alcohol is added as an antisolvent [3, 25, 26]. On the other hand, in the case of charged Si QDs dispersed in polar solvents such as methanol, a nonpolar solvent is added as an antisolvent [4]. By these size purification processes, polydispersity of the size distribution, which is defined by the standard deviation divided by the average diameter, of smaller than 10% is achieved.

In charged QDs dispersed in aqueous media, electrophoresis is another choice for the size separation. Surface-modified hydrophilic cadmium selenide (CdSe) and cadmium telluride (CdTe) QDs were size-separated by capillary electrophoresis [27-

[a] Department of Electrical and Electronic Engineering, Kobe University, 657-8501 Kobe, Japan. Email: fujii@eedept.kobe-u.ac.jp

†Electronic Supplementary Information (ESI) available: The relation between migration distance and diameter (Figure S1). Results of gel electrophoresis of LBP samples (Figure S2). Procedure to prepare TEM samples after electrophoresis (Figure S3). PL spectra after electrophoresis (Figure S4). See DOI: 10.1039/x0xx00000x

[29]. Gel electrophoresis was also applied to cadmium sulphide (CdS) QDs [30] and graphene QDs [31]. Although gel electrophoresis is not suitable for the production of large amounts of size-purified QDs, it is suitable for the study of the fundamental physics because of the high size resolution and the capability to immobilize size-separated QDs in a solid. However, despite the fact that it is a standard experimental method for separation and analysis of bio-substances such as DNA, RNA and proteins, its application to bio-compatible Si QDs is very rare[32]. In Ref. [32], gel electrophoresis is applied to blue-green luminescent Si QDs in order to study the charging states. Blue-green luminescence of Si QDs usually does not depend strongly on the size and is considered to arise from the surface states.[33, 34]. To our best knowledge, the gel electrophoresis has never been applied to Si QDs, especially the red to NIR luminescent ones, for the purpose of size separation.

In this work, we demonstrate that water-soluble hydrophilic Si QDs can be a subject of gel electrophoresis and that the high-resolution size separation is possible. As hydrophilic Si QDs, we employ boron (B) and phosphorus (P) co-doped Si QDs [35, 36]. The QDs have a very heavily B and P doped amorphous shell on the surface of a crystalline Si core [37]. The shell induces negative potential on the surface and makes the QDs dispersible in water [38]. We show that gel electrophoresis can separate B and P codoped Si QDs by size precisely, which allows us to study the size dependence of the photoluminescence energy and the spectral width in detail. We demonstrate that the luminescence of B and P codoped Si QDs is very broad even after the size-separation and that there is a universal relation between the luminescence peak energy and the spectral width.

Experimental

B and P codoped Si QDs were prepared by the procedure described in detail in our previous papers [35]. Briefly, thick Si-rich borophosphosilicate glass (BPSG) films were deposited on a stainless-steel plate by simultaneously sputtering Si, SiO_2, B_2O_3, and phosphosilicate glass (PSG) (SiO_2:P_2O_5=95:5wt%). In this work, we prepared two Si-rich BPSG films with different B and P concentrations, that is, 0.8 atom% B and 0.3 atom% P (refer to LBP), and 0.9 atom% B and 0.6 atom % P (refer to HBP). We will mainly discuss the data obtained for HBP samples unless otherwise specified. The Si-rich BPSG films were then peeled off from the stainless-steel plate and annealed in a N_2 gas atmosphere (950−1200°C) for 30 min to grow codoped Si QDs in a BPSG matrix. Finally, Si QDs were extracted from a matrix by hydrofluoric acid (HF) etching, and then transferred to methanol and stored for more than 6 days. Finally, the solvent was exchanged with distilled water (methanol concentration <1/100) [38]. Hereafter, we distinguish Si QDs samples by the growth temperature and the B and P concentrations in the precursor. For example, we refer Si QDs grown at 1050°C from HBP to HBP1050.

Native polyacrylamide gel electrophoresis (native-PAGE) was performed using a vertical electrophoresis cell (Bio-Rad, Mini-Protean Tetra System) with precast polyacrylamide gel (Bio-Rad, Mini-Protean TGX Gel (15 well, 15 μL, Any kD)) in Tris/Glycine buffer (Bio-Rad) at 100 V for 60 min. Glycerol was added to a water solution of Si QDs (Si QD solution: glycerol = 6: 1) before loading. After electrophoresis, the gel was dried by a gel dryer (Bio Craft, BC-801) at 70°C for 2-3 hours in vacuum.

Photoluminescence (PL) spectra of Si QDs in a gel were measured by using a single spectrometer equipped with a liquid N_2-cooled InGaAs diode array (OMA-V-SE, Roper Scientific) and a charge-coupled device (CCD) (Roper Scientific). The excitation wavelength and the excitation power were 405 nm and 2-7 μW, respectively.

Results and discussion

Figure 1(a) shows a water solution of Si QDs grown at 1150°C. The solution is very clear and light scattering by agglomerates is not observed. In fact, light transmittance below the band gap energy of bulk Si crystal is almost 100%. The high solution dispersibility of codoped Si QDs is due to the negative surface potential. In our previous work, we studied the zeta potential of codoped Si QDs grown at different conditions. The zeta potentials were -30–-50 mV and no clear dependence on the growth parameters was observed.[5, 6, 38]

Figure 1(b) shows a transmission electron microscope (TEM) (JEM-2100F, JEOL) image of Si QDs grown at 1150°C. For the TEM observation, the Si QD solution was dropped on a graphene-oxide-coated copper mesh [37]. No three-dimensional agglomerates are observed in the TEM image due to the perfect dispersion in methanol. The high dispersibility in polar solvents is a specific feature of B and P codoped Si QDs[38]. The high-resolution TEM image in the inset reveals that the Si QD is composed of a crystalline core and an amorphous shell[37]. The lattice spacing corresponds to {111} planes of the Si crystal. The amorphous shell is composed of B, Si and P, and the thickness depends on B and P concentrations in a precursor (Si-rich BPSG) [37]. The average diameter estimated from TEM images is 6.7 nm with the standard deviation of 1.3 nm (Figure 1(c)).

Figure 1(d) shows PL spectra of Si QDs grown at different temperatures dispersed in water. Bright and stable PL is observed in water. The PL shifts to a higher energy with decreasing the growth temperature (T_a), i.e., with decreasing the average diameter. In this growth temperature range, the average diameter is changed from 2.7 nm to 6.7 nm. In B and P codoped Si QDs, the PL energy and the quantum yield depend not only on the size, but also on the doping concentration[4, 37]. In general, increase of the doping concentration shifts the PL to lower energy.

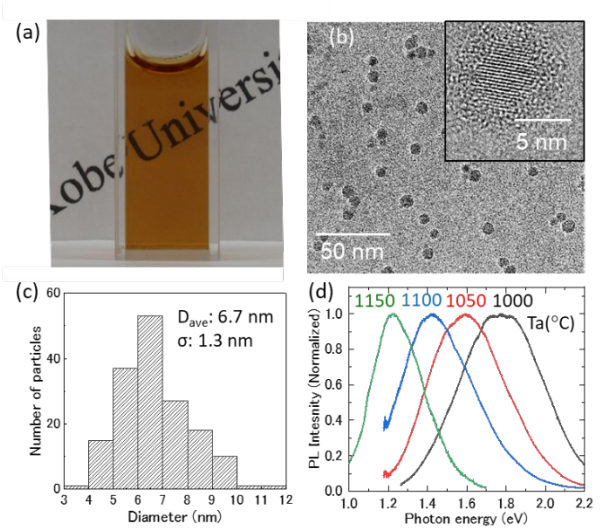

Figure 1 (a) Water solution of B and P codoped Si QDs (HBP1150). (b) TEM image of Si QDs (HBP1150). Inset is a high-resolution TEM image of a Si QD. (c) Size distribution obtained from TEM images. (d) PL spectra of Si QDs dispersed in water. The growth temperature is changed from 1000°C to 1150°C.

Figure 2 shows the results of electrophoresis of HBP samples grown at temperatures from 950°C to 1200°C (HBP950-HBP1200). For HBP1000-HBP1200, the average diameters of Si QDs estimated from TEM images are shown at the bottom of the image, while for HBP950, that estimated from the PL peak energy[5] is shown. For all the samples, we can clearly see brownish bands corresponding to Si QDs. This implies that codoped Si QDs can flow in polyacrylamide gel. The plots on the images represent the color depths obtained from the images. The relation between the peak of the color depth (peak migration distance) and the average diameter of Si QDs is shown in the Supporting Information (Figure S1). We can see that the migration distance increases with decreasing the average diameter. Furthermore, the bands spread in large migration distance ranges. These results indicate that Si QDs are successfully separated by size. Similar results are observed in LBP samples (Figure S2 in the Supporting Information), although there are some quantitative differences discussed later.

In order to confirm the successful size separation, we tried to observe Si QDs in a small region of a gel by TEM. Since the amount of Si QDs retrievable from a small region of a single well is too small for TEM observations, we performed electrophoresis for 13 wells for the HBP1150 sample and collected gels sliced in the migration distance range from 9 mm to 11 mm. The procedure is schematically shown in the Supporting Information (Figure S3). The sliced gels were then immersed in hot water (50-70°C) to extract Si QDs, and the QDs were retrieved by using a syringe filter (Sartorius, Minisart RC4). Figure 2(b) shows a TEM image of the Si QDs. The image is blurred because of residual gels surrounding Si QDs. From the first glance, we notice that the size distribution is largely improved compared to that in Figure 1(b) (before size separation), despite the fact that we sliced out quite a large gel block (2 mm in the direction of migration). The size distribution estimated from TEM images (Figure 2(c)) confirms the successful size purification. It is very plausible that the size distribution can be further improved if we sliced out a smaller block. Measuring luminescence spectra of a small region is practically equivalent to slice out a small block.

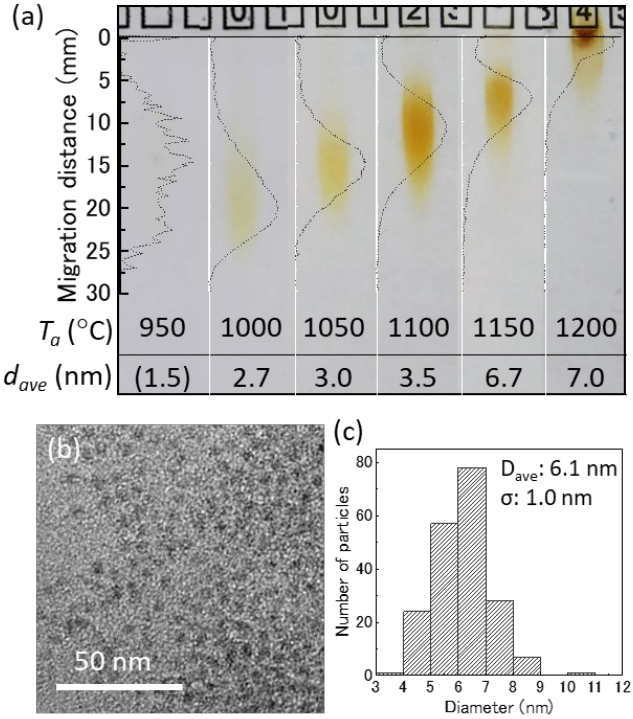

Figure 2 Electrophoresis of Si QDs (HBP). The growth temperature (T_a) is changed from 950°C to 1200°C. The average diameter of Si QDs estimated from TEM images are shown in the figure (HBP1000-HPB1200). The size of the HBP950 sample is estimated from the PL peak energy. (b) TEM image of Si QDs retrieved from gel in a well of HBP1150 in the migration distance range from 9 mm to 11 mm. (c) Size distribution obtained from TEM images of Si QDs retrieved from gel.

Figure 3(a) shows a luminescence image of the gel in Figure 2 (HBP samples) under UV light irradiation. The data of LBP samples are shown in the Supporting Information (Figure S2). Bright reddish luminescence is observed in the whole regions in HBP950-HBP1050 samples. Although it is not easy to recognize in the picture, the emission color changes from red to orange from the top to the bottom. In HBP1100, red luminescence is observed only in the lower half region. In HBP1150 and HBP1200, luminescence is not observed. As will be shown later, the appearance of the dark regions is simply due to low sensitivity of the camera in a long wavelength range. Figure 3b shows PL spectra of HBP1100 obtained at different positions of the gel (from 9 mm to 24 mm with 1 mm step). The spot size for the PL excitation is about 200 μm. We can clearly see that the PL peak shifts from 1.2 eV to 1.8 eV with increasing the migration distance. Therefore, a PL spectrum of a Si QDs solution with the maximum around 1.4 eV is divided into 16 spectra with the maxima extended from 1.2 eV to 1.8 eV. In the left end of the graph, we can clearly distinguish the two spectra (black and red). The difference of the peak energies is ~12 meV. Considering the relation between the PL peak energy and the average diameter of codoped Si QDs obtained previously,[4] the

12 meV difference in this wavelength range corresponds to the diameter difference of ~0.1 nm. Although this value has no physical meaning, it indicates that precise size separation can be achieved by the gel electrophoresis. In Figure 3(b), despite the size purification, the spectral width is very large, especially at the high energy range. We will discuss the relation between the peak energy and the width of the PL spectra later. The PL spectra obtained for all other samples are summarized in the Supporting Information (Figure S3).

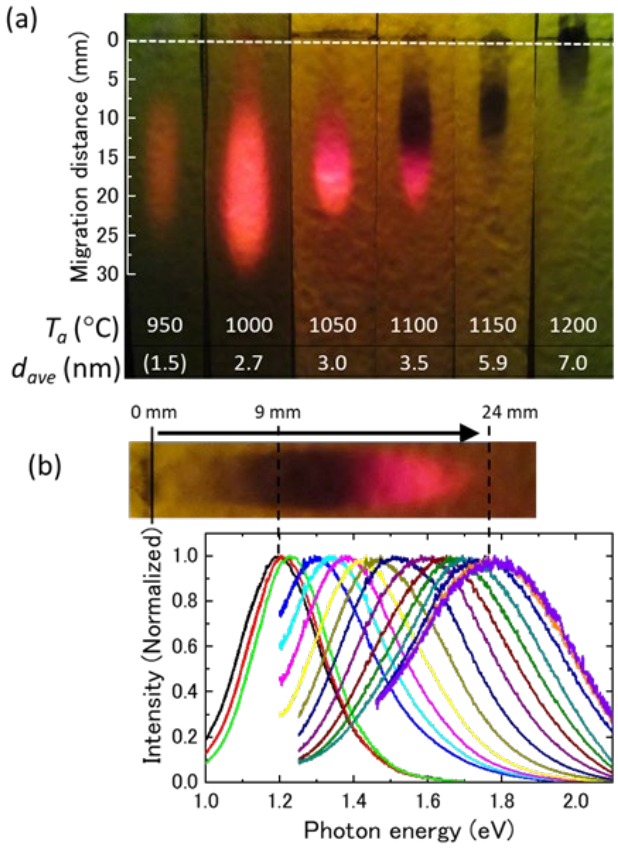

Figure 3 (a) Luminescence images of the gel in Figure 2 under UV light irradiation. The excitation light is cut by a long pass filter (425nm and 575 nm). (b) Luminescence image of HBP1100 and the PL spectra obtained at different positions (9mm to 24 mm) in the gel.

Figure 4(a) shows the relation between the PL peak energy and the migration distance obtained for HBP samples grown at different temperatures (HBP1000-HBP1150). The relation is not universal but depends on the growth temperature. This means that QD size is not a single parameter to determine the migration distance and the PL peak energy. If we assume that the PL peak energy is solely determined by the size, Figure 4(a) indicates that different-temperature-grown-Si QDs have different surface charges even if the size is the same. On the other hand, if we assume that the migration distance is determined solely by the size, different-temperature-grown-Si QDs exhibit PL at different energies even if the size is the same. Distinction of the two scenarios is not possible within the present work. However, most probably, both the surface charges and the PL energy depend on the growth temperature, i.e., doping affects both the surface structure and optical properties of Si QDs.

In the Supporting Information (Figure S2(c)), we show the data obtained for LBP samples. The data are similar to those obtained for HBP samples (Figure 4(a)). However, there are quantitative differences. In particular, the migration distance of LBP samples is, on the whole, smaller than that of HBP samples, while the PL peak energy of LBP samples is, on the whole, larger than that of HBP samples. These differences indicate that the surface charges and the PL peak energy depend also on the B and P concentration in a precursor. In order to further clarify the effects of doping on the structural and optical properties of Si QDs, 2-dimensional electrophoresis, in which molecules are separated linearly according to their isoelectric points in the first dimension, and then they are separated according to the molecular weights in the second dimension, may be useful.

Figure 4(b) summarizes the relation between the PL spectral width (full width at half maximum: FWHM) and the peak energy of HBP and LBP samples grown at different temperatures obtained at different migration distances. Although the data are scattered, we can see a clear trend; FWHM increases with increasing the PL peak energy. The data are similar to those of codoped Si QDs size-purified by a size-selective precipitation method[4]. In Figure 4(b), we also plot the data of undoped Si QDs taken from Ref. [3]. In undoped Si QDs, the PL FWHM also increases with increasing the PL peak energy. This trend is probably due to stronger confinement of excitons in smaller Si QDs and resultant stronger coupling with phonons[39]. The larger PL FWHM of codoped Si QDs than that of undoped ones indicates that excitons are further localized in codoped Si QDs due to the existence of charged impurities[40].

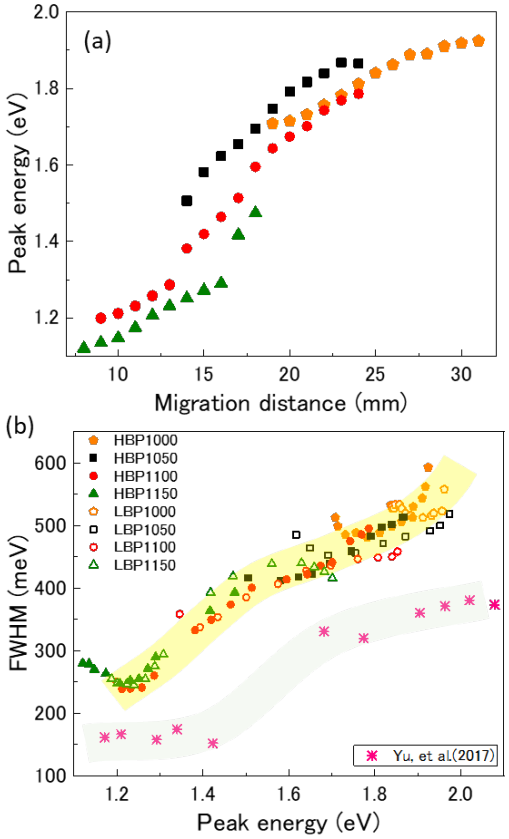

Figure 4 (a) PL peak energy as a function of migration distance obtained for HBP samples. (b) PL FWHM as a function of PL peak energy obtained for HBP and LBP samples. The data of undoped Si QDs taken from Ref. [3] are also shown.

Conclusions

Gel electrophoresis was applied for the first time to Si QDs and the high-resolution size separation was achieved. The capability of gel electrophoresis to immobilize size-separated Si QDs in a solid matrix makes detailed analyses of size-purified Si QDs possible. PL studies of dried gels demonstrated that a broad PL spectrum of a Si QDs solution can be separated into more than 15 spectra of size-purified Si QDs. The present results indicate that a gel electrophoresis is a powerful tool for separation and analysis of water-dispersible Si QDs and for the development of Si QDs-based nanocomposite materials, such as Si QDs-metal nanocomposites[41] and Si QDs-antibody composites[11].

Conflicts of interest

There are no conflicts to declare.

Acknowledgements

This work was partly supported by JSPS KAKENHI grant numbers 16H03828, 18K14092, 18KK0141 and 19K22111, and JSPS 2018 Bilateral Joint Research Projects (Japan–Australia).

References

1. L. Mangolini and U. Kortshagen, *Adv. Mater.*, 2007, **19**, 2513–2519.
2. F. Sangghaleh, I. Sychugov, Z. Yang, J. G. C. Veinot and J. Linnros, *ACS nano*, 2015, **9**, 7097-7104.
3. Y. Yu, G. Fan, A. Fermi, R. Mazzaro, V. Morandi, P. Ceroni, D.-M. Smilgies and B. A. Korgel, *J. Phys. Chem. C*, 2017, **121**, 23240-23248.
4. H. Sugimoto, M. Yamamura, R. Fujii and M. Fujii, *Nano Lett.*, 2018, **18**, 7282-7288.
5. H. Sugimoto, M. Fujii, K. Imakita, S. Hayashi and K. Akamatsu, *J. Phys. Chem. C*, 2013, **117**, 11850-11857.
6. L. Ostrovska, A. Broz, A. Fucikova, T. Belinova, H. Sugimoto, T. Kanno, M. Fujii, J. Valenta and M. H. Kalbacova, *Rsc Advances*, 2016, **6**, 63403-63413.
7. T. Belinova, L. Vrabcova, I. Machova, A. Fucikova, J. Valenta, H. Sugimoto, M. Fujii and M. Hubalek Kalbacova, *physica status solidi (b)*, 2018, **255**, 1700597.
8. S. Bhattacharjee, I. M. C. M. Rietjens, M. P. Singh, T. M. Atkins, T. K. Purkait, Z. Xu, S. Regli, A. Shukaliak, R. J. Clark, B. S. Mitchell, G. M. Alink, A. T. M. Marcelis, M. J. Fink, J. G. C. Veinot, S. M. Kauzlarich and H. Zuilhof, *Nanoscale*, 2013, **5**, 4870-4883.
9. M. A. Islam, R. Sinelnikov, M. A. Howlader, A. Faramus and J. G. C. Veinot, *Chem. Mater.*, 2018, DOI: 10.1021/acs.chemmater.8b04227.
10. C. J. T. Robidillo, M. Aghajamali, A. Faramus, R. Sinelnikov and J. G. C. Veinot, *Nanoscale*, 2018, DOI: 10.1039/C8NR05368E.
11. H. Yanagawa, A. Inoue, H. Sugimoto, M. Shioi and M. Fujii, *MRS Communications*, 2019, **9**, 1079-1086.
12. F. Meinardi, S. Ehrenberg, L. Dhamo, F. Carulli, M. Mauri, F. Bruni, R. Simonutti, U. Kortshagen and S. Brovelli, *Nature Photonics*, 2017, **11**, 177.
13. A. Marinins, R. Zandi Shafagh, W. van der Wijngaart, T. Haraldsson, J. Linnros, J. G. C. Veinot, S. Popov and I. Sychugov, *ACS Appl Mater Interfaces*, 2017, **9**, 30267-30272.
14. E. J. Henderson, J. A. Kelly and J. G. C. Veinot, *Chem. Mater.*, 2009, **21**, 5426-5434.
15. M. L. Mastronardi, F. Hennrich, E. J. Henderson, F. Maier-Flaig, C. Blum, J. Reichenbach, U. Lemmer, C. Kübel, D. Wang, M. M. Kappes and G. A. Ozin, *Journal of the American Chemical Society*, 2011, **133**, 11928-11931.
16. X. Liu, Y. Zhang, T. Yu, X. Qiao, R. Gresback, X. Pi and D. Yang, *Particle & Particle Systems Characterization*, 2016, **33**, 44-52.
17. A. R. Van Sickle, J. B. Miller, C. Moore, R. J. Anthony, U. R. Kortshagen and E. K. Hobbie, *ACS Appl. Mater. Interfaces*, 2013, **5**, 4233-4238.
18. S. L. Brown, J. B. Miller, R. J. Anthony, U. R. Kortshagen, A. Kryjevski and E. K. Hobbie, *ACS nano*, 2017, **11**.
19. J. B. Miller, A. R. Van Sickle, R. J. Anthony, D. M. Kroll, U. R. Kortshagen and E. K. Hobbie, *ACS nano*, 2012, **6**, 7389-7396.
20. L. Bai, X. Ma, J. Liu, X. Sun, D. Zhao and D. G. Evans, *J Am Chem Soc*, 2010, **132**, 2333-2337.
21. A. L. Rogach, D. V. Talapin, E. V. Shevchenko, A. Kornowski, M. Haase and H. Weller, *Adv. Funct. Mater.*, 2002, **12**, 653-664.

22. A. Raevskaya, V. Lesnyak, D. Haubold, V. Dzhagan, O. Stroyuk, N. Gaponik, D. R. T. Zahn and A. Eychmüller, *J. Phys. Chem. C*, 2017, **121**, 9032-9042.
23. S. Komada, T. Kobayashi, Y. Arao, K. Tsuchiya and Y. Mori, *Adv. Powder Technol.*, 2012, **23**, 872-877.
24. A. A. Guzelian, J. E. B. Katari, A. V. Kadavanich, U. Banin, K. Hamad, E. Juban, A. P. Alivisatos, R. H. Wolters, C. C. Arnold and J. R. Heath, *The Journal of Physical Chemistry*, 1996, **100**, 7212-7219.
25. M. L. Mastronardi, F. Maier-Flaig, D. Faulkner, E. J. Henderson, C. Kubel, U. Lemmer and G. A. Ozin, *Nano Lett.*, 2012, **12**, 337-342.
26. W. Sun, C. Qian, L. Wang, M. Wei, M. L. Mastronardi, G. Casillas, J. Breu and G. A. Ozin, *Adv. Mater.*, 2015, **27**, 746-749.
27. C. Carrillo-Carrion, Y. Moliner-Martinez, B. M. Simonet and M. Valcarcel, *Analytical chemistry*, 2011, **83**, 2807-2813.
28. Y. Q. Li, H. Q. Wang, J. H. Wang, L. Y. Guan, B. F. Liu, Y. D. Zhao and H. Chen, *Anal Chim Acta*, 2009, **647**, 219-225.
29. X. Song, L. Li, H. Qian, N. Fang and J. Ren, *Electrophoresis*, 2006, **27**, 1341-1346.
30. A. Eychmueller, L. Katsikas and H. Weller, *Langmuir*, 1990, **6**, 1605-1608.
31. F. Zhang, F. Liu, C. Wang, X. Xin, J. Liu, S. Guo and J. Zhang, *ACS Appl Mater Interfaces*, 2016, **8**, 2104-2110.
32. B. A. Manhat, A. L. Brown, L. A. Black, J. B. Ross, K. Fichter, T. Vu, E. Richman and A. M. Goforth, *Chemistry of materials : a publication of the American Chemical Society*, 2011, **23**, 2407-2418.
33. R. Sinelnikov, M. Dasog, J. Beamish, A. Meldrum and J. G. C. Veinot, *ACS Photonics*, 2017, **4**, 1920-1929.
34. M. Dasog, G. B. De los Reyes, L. V. Titova, F. A. Hegmann and J. G. Veinot, *ACS nano*, 2014, **8**, 9636-9648.
35. M. Fujii, H. Sugimoto and K. Imakita, *Nanotechnology*, 2016, **27**, 262001.
36. M. Fujii, H. Sugimoto and S. Kano, *Chem. Commun.*, 2018, **54**, 4375-4389.
37. H. Sugimoto, M. Yamamura, M. Sakiyama and M. Fujii, *Nanoscale*, 2018, **10**, 7357-7362.
38. H. Sugimoto, M. Fujii, Y. Fukuda, K. Imakita and K. Akamatsu, *Nanoscale*, 2014, **6**, 122-126.
39. B. Somogyi, E. Bruyer and A. Gali, *The Journal of Chemical Physics*, 2018, **149**, 154702.
40. F. Iori and S. Ossicini, *Physica E*, 2009, **41**, 939-946.
41. A. Inoue, H. Sugimoto and M. Fujii, *Rsc Advances*, 2019, **9**, 15171-15176.